A Relativistic Magnetron Operated With Permanent Magnets

Yakov E. Krasik, *Senior Member, IEEE*, John G. Leopold, and Uri Dai

***Abstract*— The results of an experimental and a numerical study of a relativistic A6 magnetron with single radial microwave power output slot operating with angular segment (AS) NdFeB permanent magnets placed inside the anode vanes and cylindrical rod magnets inside the cathode are presented. With permanent magnets, $\sim 10^{-7}$ s long pulses of tens of megawatts of microwave power with an electronic efficiency of ∼7% are generated. The results of experiments and simulations show that electron losses near the poles of the anode magnets where magnetic field lines cross the anode-cathode gap limit the microwave generation efficiency.**

***Index Terms*— High power microwaves (HPM), permanent magnets, relativistic magnetron.**

I. Introduction

ONE of the most attractive high power microwave (HPM) source is the relativistic magnetron which can generate hundreds of megawatts of power, up to several hundreds of nanoseconds long pulses in the *S*- and *L*-bands [1], [2]. A common source of electrons for this type of magnetron is an explosive emission plasma [3] formed at the surface of the cathode when an accelerating high voltage (HV) pulse is applied to the coaxial cathode-resonator structure. Electrons, emitted from the surface of this plasma, experience azimuthal drift in the crossed radial electric and applied static axial magnetic field, B_z. The latter should be sufficiently high above the Hull cutoff magnetic field, and the drift velocity should be close to the phase velocity of the electromagnetic wave in the anode resonators. When these conditions are satisfied, part of the electrons, namely those synchronized with the phase velocity will transfer their potential energy to the wave and experience drift toward the anode in $B_z \times E_\Theta$, where E_Θ is the wave azimuthal electric field. The extraction of the microwave power is either in the radial direction through open axial slots in one or more cavities of the anode resonators coupled to waveguides or in the axial direction using a diffraction output coupled with an antenna.

One of the main advantages of relativistic magnetrons is their narrow microwave bandwidth (tens of megahertz) and high efficiency (up to 70%) of energy transfer from the drifting electron flow to microwave power [4]. On the other hand, there are some disadvantages limiting its broad application. Namely, the cathode explosive plasma can be axially and azimuthally nonuniform which results in nonuniform electron emission. Plasma instabilities may lead to cathode-anode gap shorting, accompanied by the deterioration of the vacuum, limiting the repetition rate of the magnetron operation. Electron impact processes can damage the anode vanes and affect vacuum too. Also, because of the coaxial geometry of the anode and cathode electrodes, it is almost impossible to satisfy conditions of equality between the wave and drifting electron velocities in the entire anode-cathode gap. Some of these features lead to frequency shifts and mode competition during the microwave generation and to a pulse shorting effect decreasing the efficiency of the magnetron operation.

Recent research showed that some of these disadvantages can be solved. Namely, the efficiency of relativistic magnetron operation can be significantly improved using transparent cathodes which results in increased coupling of the azimuthal electric field of the wave with the drifting electrons [5]. Also, one can apply an active plasma source to avoid the disadvantages related to explosive emission plasmas [6]. Mode competition and frequency drift can be avoided using coupling between resonator cavities [7], and the damage to the anode caused by electron flow can be minimized by building the anode block with modern hard alloy materials.

However, one of the main factors which influence the total efficiency of a relativistic magnetron operation is the necessity of an intense (up to 2 T) external magnetic field produced either by a pulsed solenoid or by Helmholtz coils which require tens of kilowatt of extra electrical power. This power is more than ten times larger than the average power required by the magnetron itself. In certain cases, there is a need to cool the coil which adds to the system's power requirements. The power needed to produce the magnetic field, coil cooling, and operation of the vacuum pumps can reduce the system's operating efficiency to <1% and increase the weight, size, and final cost of the complete system.

The external Helmholtz coils were replaced by electromagnets [8] which reduce the dimensions of the magnetron system to some extent. Relatively large and heavy permanent magnets were considered when operating magnetrons with diffraction output [9]–[11] to produce an axial magnetic field of ∼0.3 T. Using this design, generation of up to 1 GW, 75-ns microwave pulses was reported in [9]. In [12], rod-shaped permanent magnets were inserted inside cylindrical slots drilled in the anode vanes of an *S*-band magnetron with a single radial

Manuscript received April 4, 2019; revised May 10, 2019 and June 1, 2019; accepted June 27, 2019. Date of publication July 18, 2019; date of current version August 9, 2019. The review of this paper was arranged by Senior Editor D. A. Shiffler. *(Corresponding author: Yakov E. Krasik.)*

Y. E. Krasik and J. G. Leopold are with the Department of Physics, Technion-Israel Institute of Technology, Haifa 3200003, Israel (e-mail: fnkrasik@physics.technion.ac.il; leopoldjg@physics.technion.ac.il).

U. Dai is with the Department of Defence Research & Development (DDR&D)/Israel Ministry of Defense (IMOD), Tel Aviv 61909, Israel (e-mail: uri_dai@mod.gov.il).

Color versions of one or more of the figures in this paper are available online at http://ieeexplore.ieee.org.

Digital Object Identifier 10.1109/TPS.2019.2926535

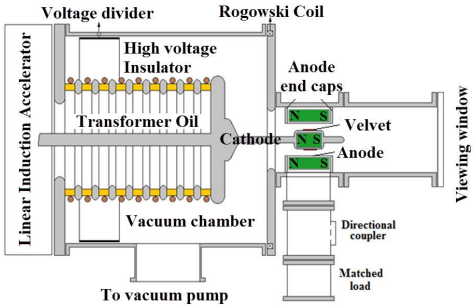

Fig. 1. Experimental setup. Green rectangles: permanent magnets.

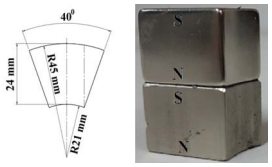

Fig. 2. Dimensions and external view of AS magnets.

output. In this paper, using numerical simulations of the magnetic field for a 12-resonator *S*-band magnetron, it was shown that with modern permanent magnets one can achieve magnetic induction necessary for electron magnetization for the applied voltage $\leq$250 kV.

In this paper, the results of experimental and numerical studies of an *S*-band A6 relativistic magnetron with a single radial output and permanent magnets installed into the anode block and the cathode electrode will be reported and discussed.

II. Experimental Setup

Experiments were carried out using a relativistic *S*-band A6 magnetron powered by a linear induction accelerator (LIA) of $\sim$100-Ω internal impedance [13]. In the present research, the LIA was operated with a decreased amplitude ($\leq$250 kV) of the negative polarity high voltage (HV) pulse. The HV pulse duration was $\sim$150 ns at full-width half-maximum (FWHM) with a rise time of $\sim$30 ns. The waveforms of voltage and output current were measured using a capacitive voltage divider and a self-integrated Rogowski coil, respectively (see Fig. 1), and were acquired by an Agilent Infiniium DS080404B (4 GHz, and 40 GS/s) digitizing oscilloscope.

Angular segment (AS) magnets (Fig. 2) were manufactured by YY Magnetics (http://www.smi-mag.com). The magnets were covered by a few micron thick Ni layer. In addition, a 150-μm thick copper foil was used to cover the magnets to prevent electron damage. A special tool was manufactured and used to place the six ASs distributed in azimuthal symmetry inside an external brass tube and fixed between two anode endcaps which are full rings with the same inner radius of 21 mm as the inner radius of the vanes, covering the resonator ends (see Fig. 2). The spaces between the ASs served as anode resonators [see Fig. 3(a) and (b)]. The external tube has a single 14 mm $\times$ 70 mm rectangular azimuthal opening located in one of the resonators. Through this slot, the microwave power is released into a rectangular waveguide

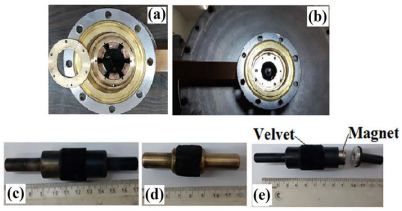

Fig. 3. External view of (a) anode with the AS magnets and the anode endcap are seen separately. (b) Same as (a), but with the cathode and the anode endcap installed. (c) Long cathode without inserted rod magnets. (d) Short cathode with rod magnets inserted. (e) Same as (c), but with inserted rod magnets.

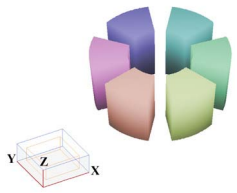

Fig. 4. 3-D drawing of the six AS magnets used in the magnetic field calculations. The orientation of the structure in the coordinate space is designated within the small box at the left hand lower corner of the drawing.

(34 mm $\times$ 72 mm) coupled to a 42-dB coupler and a matched load (see Fig. 1) [14].

In experiments, several types of cylindrical cathodes with diameters of 18–20 mm and lengths of 20–100 mm made either of stainless steel or aluminum or brass tubes with a wall thickness of 1 mm with and without inserted N52 magnets were tested. In most experiments, velvet strips of various lengths were glued to the cathode surface and served as the emitting surface [Fig. 3(c)–(e)]. In some of the experiments, the nonemitting surfaces of cathodes made of aluminum were coated by 90-μm thick hard Aluminum oxide to protect them from explosive emission spots.

We measured the axial magnetic field for the six AS arrangement using a Hall-based sensor connected to the Gauss meter 915 (Magnetic Instrumentation, htpps://maginst.com/) and placed 4 mm below their inner radius. We also calculated the magnetic field for the arrangement seen in Fig. 4 using the Field Precision 3-D MAGNUM magneto-static code (https://www.fieldp.com/magnum.html). Because of the final size of the magnetic field measuring probe, we could not measure the radial variation of the magnetic field, but calculations show that the axial magnetic field varies $\leq$2% radially in the gap between the cathode and the anode.

In Fig. 5, we compare the measured and calculated values of B_z. To make the calculated B_z values fit the measured data (Fig. 5), we had to use the remanence magnetic flux density $B_R = 1.2$ T, rather than a value in the range 1.43–1.48 T provided by the manufacturer for the purchased N52 AS magnets, that is, our permanent magnets are relatively weak. We calibrated B_R by measuring the magnetic field near rod magnets used inside the cathode and we found the same remanence value. We also measured arrangements containing anode and cathode magnets, and for all arrangements, the calibration was confirmed.

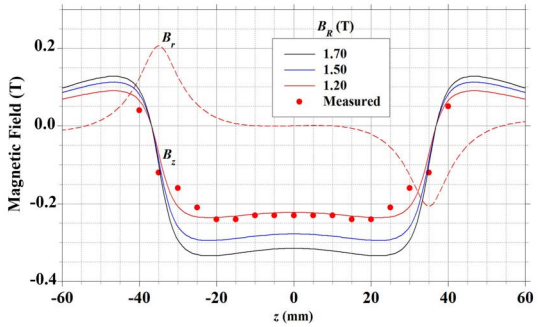

Fig. 5. Comparison of the measured (●) and MAGNUM calculated (red solid line for B_R = 1.2 T) values of the axial magnetic field, B_z, at $r = 17$ mm for an arrangement of six 70-mm long AS magnets for different values of the remanence magnetic flux density, B_R. For $B_R = 1.2$ T, we draw the radial magnetic field B_r along the same axial line (red dashed line).

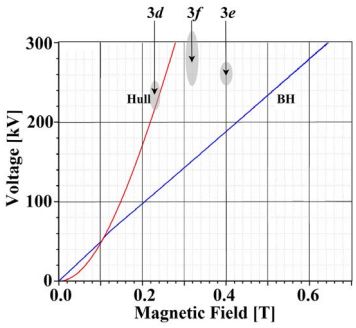

Fig. 6. BH condition and Hull cutoff magnetic field dependences for the magnetron operating at a frequency of 2.85 GHz and for the anode and cathode radii of 2.1 and 1.1 cm, respectively. Shadowed regions: experiments described in the respective subsections 3*d*, 3*e*, and 3*f*.

The Hull cutoff magnetic field and the Buneman–Hartree (BH) limit (see, for example, Fig. 6 for 2.85-GHz resonance frequency) for most of our experiments is 200–250 kV; the magnetic field produced by only six 70-mm long AS magnets seems to be above the Hull limit, but only along the central ~50-mm long region where the axial magnetic field is nearly constant (Fig. 6).

In order to get closer to the BH limit with only AS magnets, B_R needs to be higher up to unrealistic values (see Fig. 5 for $B_R = 1.5$ and 1.7 T). As the AS magnet length is decreased, the magnetic field increases but over a shorter range. Adding a cathode magnet of the same pole orientation as the anode magnet, increases B_z but not overall, and the formation of intense magnetic vector lines pointing in the radial direction at the poles of the magnets has to be taken into account when choosing the length of the emission surface l_e.

The resonance frequencies of the magnetron anode resonators in the presence of various cathodes were measured using a Network analyzer (Rohde and Schwarz—ZVL 9 kHz–6 GHz) by determining the minimum of the reflection coefficient S_{11} of the electromagnetic wave reflected from the anode slot. It was found that depending on the cathode design, the resonance frequencies changed in the range 2.503–3.649 GHz. In Fig. 7, one can see an example of such measurements of the resonance frequency of the magnetron anode with AS magnets and a 21-mm diameter cathode.

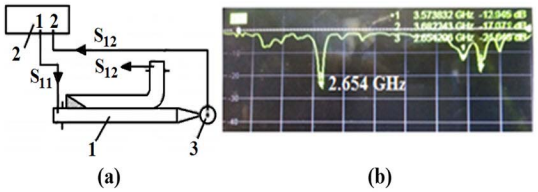

Fig. 7. (a) Setup for resonance frequency measurements: 1) directional coupler; 2) network analyzer; and 3) anode with an inserted cathode. (b) Frequency response of the magnetron's resonators for an anode with AS magnets and a 21-mm cathode.

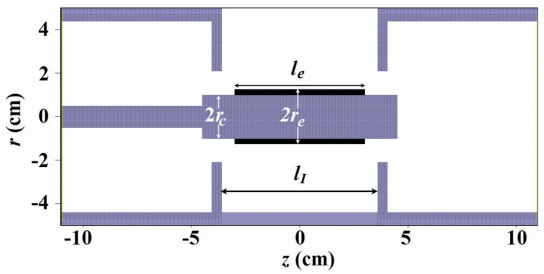

Fig. 8. Geometry of the simulated magnetron with a cathode radius r_c. The anode radius was 21 mm, the slot radius 44 mm, and interaction length, $l_I = 72$ mm. The emitting black velvet is of radius r_e and length l_e. In this slice of the geometry, the open slot connected to a conical antenna is seen at the top and the opposite closed resonator slot at the bottom, both limited by anode caps.

III. Experimental Results and Simulations

A. PIC Simulations for Constant Axial Magnetic Fields

The relativistic A6 magnetron with a single radial output discussed in this paper falls in the category studied by us in [15], that is, a magnetron with its six axial resonators covered at the two ends with conducting endcaps. For the magnetron studied in [15], MAGIC simulations found that the axial electron current plays a significant role in balancing the input power and the microwave power. Moreover, by changing the length of the emitting region on the cathode, one could affect this balance and optimize the output power. We also found that decreasing the axial current while increasing the magnetron current does not necessarily lead to microwave power increase. These simulations have not been experimentally confirmed so far.

We perform MAGIC-particle in cell (PIC) [16] simulations of the magnetron operation in the same manner as explained in detail in [15]. We study first, a magnetron with geometry as that seen in Fig. 8 applying a constant uniform axial magnetic field B_z in the entire simulation volume. The voltage rising in 10 ns to a fixed value of ~220 kV is applied on the upstream boundary in Fig. 8, which produces a total current of ~2.3 kA. In the experiments, the voltage rise time is much longer, so one should note that when a simulation time is mentioned, it should be compared to the experiment at the same time interval following the rise time.

In Fig. 9, we present the time dependence of the microwave power for $r_c = 11.5$ mm, $r_e = 12.5$ mm, and $l_e = 60$ mm. In Fig. 9(a), the axial magnetic field is 0.31 T, whereas in Fig. 9(b), it is 0.35 T. For 0.4 T, the microwave power becomes negligible, which means that the BH limit is close

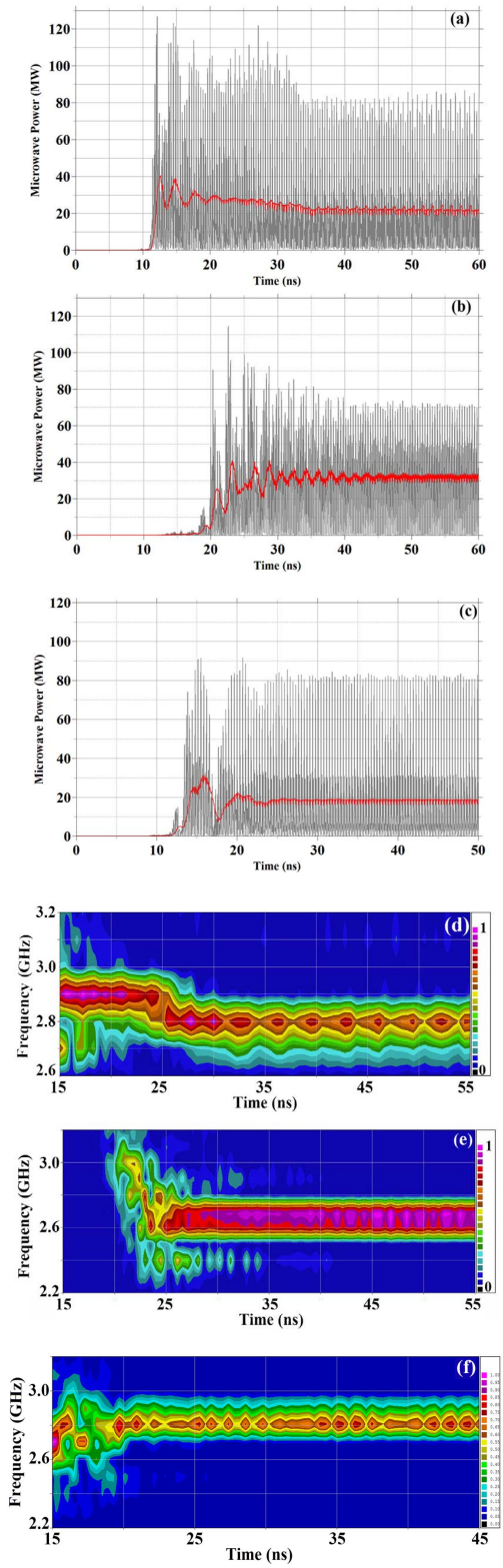

Fig. 9. Results of MAGIC simulations for a constant axial magnetic field. The instantaneous (gray) and mean (red) microwave power for (a) $B_z = 0.31$ T and (b) 0.35 T for the geometry of Fig. 8 and $l_e = 60$ mm, and the corresponding frequency–time contours in (d) for (a) and in (e) for (b). In (c), $B_z = 0.31$ T and $l_e = 20$ mm. (f) Frequency–time analysis for the case in (c).

(see Fig. 6). As the axial magnetic field increases, it takes longer for the microwaves to switch on and mode competition is discerned before a fixed frequency mode forms. In Fig. 9(d), for 0.31 T, the initial frequency is ∼2.9 GHz which then shifts to ∼2.8 GHz. For 0.35 T, the frequency is first near ∼3 GHz and settles on ∼2.7 GHz [Fig. 9(e)]. In Fig. 9(c), for $B_z = 0.31$ T and $l_e = 20$ mm, the frequency settles at ∼2.8 GHz [Fig. 9(f)]. We can state that for this magnetron and the conditions chosen, instabilities may develop due to mode competition and the instantaneous output power can reach values up to ∼100 MW, with >20% efficiency (relative to the input power).

In all our simulations, we use a matched long conical continuation of the open slot's rectangular cross section. For some cases, we also simulated the same magnetrons with the waveguide arrangement (see Fig. 1) replacing the conical antenna. For all cases where we compared these two arrangements, the calculated power at the exit of a matched antenna is larger by a factor of ∼2.2 compared to the power radiated when a model of the experimental arrangement was used. The latter occurs because the transition region between the load and the open resonator is not smooth, causing partial reflection of the electromagnetic wave. Because of this, we assume that the experimentally measured power is smaller by this factor when compared to the simulated values for a matched long conical continuation of the open slot's rectangular cross section.

These calculations suggest that when permanent magnets are considered, it is required that these produce an axial magnetic field of $0.31\ \text{T} \leq B_z < 0.4\ \text{T}$ to obtain the same magnetron power as above.

B. Introducing Permanent Magnets

To obtain such magnetic fields, we need to consider AS magnets with artificial remanence magnetic flux density $B_R \geq 1.5$ T (see Fig. 5). Nonetheless, we simulated the above magnetron with such imaginary permanent magnets. The output microwave power for this case is a few kilowatt at most.

The reason for this is seen in Fig. 10(a) and (b), where the electrons' positions are drawn in the coordinate space of various slices in the magnetron geometry for six 70-mm long AS magnets of $B_R = 1.7$ T (Figs. 4 and 5). These are compared to when a fixed magnetic field is utilized [Fig. 10(c) and (d)]. For a fixed magnetic field, the electron current splits into the magnetron current and an axial current $I_T = I_M + I_A$, where I_T, I_M, and I_A are the total, magnetron, and axial currents, respectively [15]. We have shown that the system behaves as two impedances connected in parallel so that $Z_T = 1/Z_M + 1/Z_A$, where Z_T, Z_M, and Z_A are the total, magnetron, and axial impedances, respectively. This allows the magnetron to shed current into axial current when it is unable to use all its current as magnetron current. For the case seen in Fig. 10(c) and (d) (fixed axial magnetic field), the voltage is ∼225–250 kV, $I_M \approx 1.2$ kA, and $I_A \approx 1.1$ kA (0.7 kA downstream and 0.4 kA upstream), that is, only about half of the total current is interacting in the resonator cavities sufficient to produce the power seen in Fig. 9(c).

For 70-mm long AS permanent magnets with $B_R = 1.7$ T, the axial magnetic field decreases and the radial magnetic field increases near the two longitudinal ends of the magnetron interaction region (Fig. 5). In Fig. 10(a) and (b), we see that because of this, the axial current, which is now under the effect

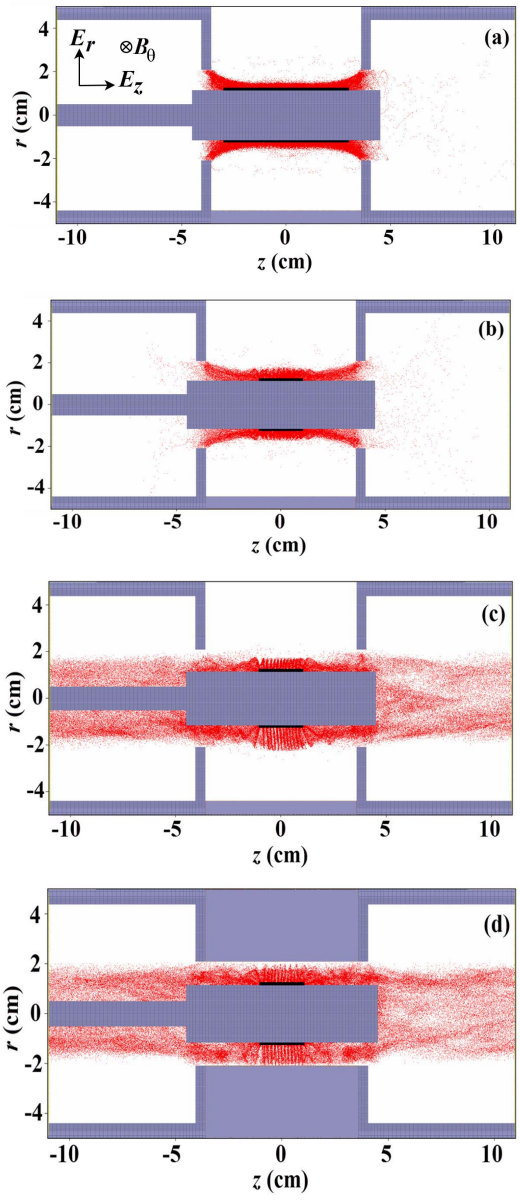

Fig. 10. PIC calculated electron positions along the flat top of the voltage pulse 40 ns after the 10 ns rise time of the voltage in the coordinate space along a [z, r] plane slicing through the (a)–(c) open magnetron slot and (d) plane through two opposite vanes. In (a) ($l_e = 60$ mm) and (b) ($l_e = 20$ mm), six 70-mm long AS permanent magnets with $B_R = 1.7$ T are used. In (c) and (d), $l_e = 20$ mm and the magnetic field is fixed at 0.31 T.

of E_r and B_r, is collected on the anode caps instead of leaving the interaction region. The corresponding space charge buildup leads to the appearance of an electric field E_z, which affects the electron drift orientation because of $E_z \times B_\varphi$ (where B_φ is the azimuthal self-magnetic field of the magnetron current) directed in an opposite direction to the $E_r \times B_z$ drift. This forces the magnetron to become a single impedance which affects the power flow in such a way that the magnetron power decreases, and for this case, to negligible values.

C. Experiments Only With AS Permanent Magnets

For our six AS magnets ($B_R = 1.2$ T), the axial magnetic field in the interaction region reaches only ~0.23 T (Fig. 5), which is slightly above the Hull limit (Fig. 6), and we should

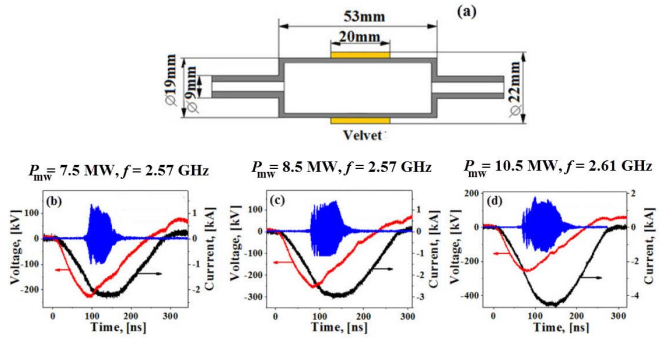

Fig. 11. (a) Geometry of the cathode used in the experiment. Six AS magnets are present and no magnet is inserted in the cathode. The velvet emitter length $l_e = 20$ mm. Waveforms of the current, voltage, and mw pulse for (b) $\varphi_{ch} = 1.5$ kV, (c) 1.9 kV, and (d) 2.3 kV.

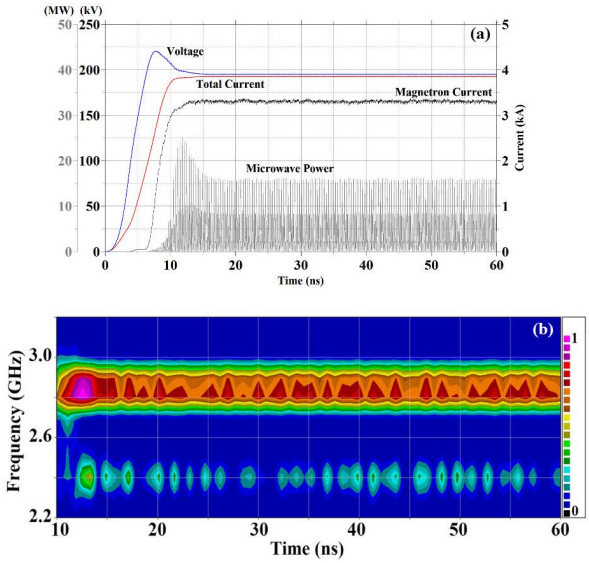

Fig. 12. (a) PIC calculated time dependence of the voltage, total and magnetron currents, and the mw power versus time. (b) Frequency–time analysis of the electric field at the edge of the conical antenna for the experimental conditions as in Fig. 11.

expect lower powers than in Fig. 9. It should be noted though that, at the same time, the radial component of the magnetic field at the pole locations is reduced too (the maximum value of $B_r \approx 0.2$ T for $B_R = 1.2$ T (Fig. 5), whereas $B_r \approx 0.3$ T for $B_R = 1.7$ T).

We performed experiments with only the six AS magnets present for the cathode seen in Fig. 3(c) and drawn in Fig. 11(a). The experimental results for increasing charging voltage, φ_{ch}, of the LIA are presented in Fig. 11(b)–(d)).

Note, in Fig. 11, that the measured voltage applied on the magnetron and the radiated ~80-ns long microwave power (7.5–10 MW) are almost independent of the charging voltage, but the current increases considerably. A small (~1.14) increase in the applied voltage in spite of ~1.53 increase in the charging voltage is related to the ~100 Ω internal impedance of the LIA and a significant decrease in the magnetron impedance because of additional electron losses between the cathode structure and the anode. We shall discuss this below.

We simulated this experiment and obtained the results seen in Fig. 12.

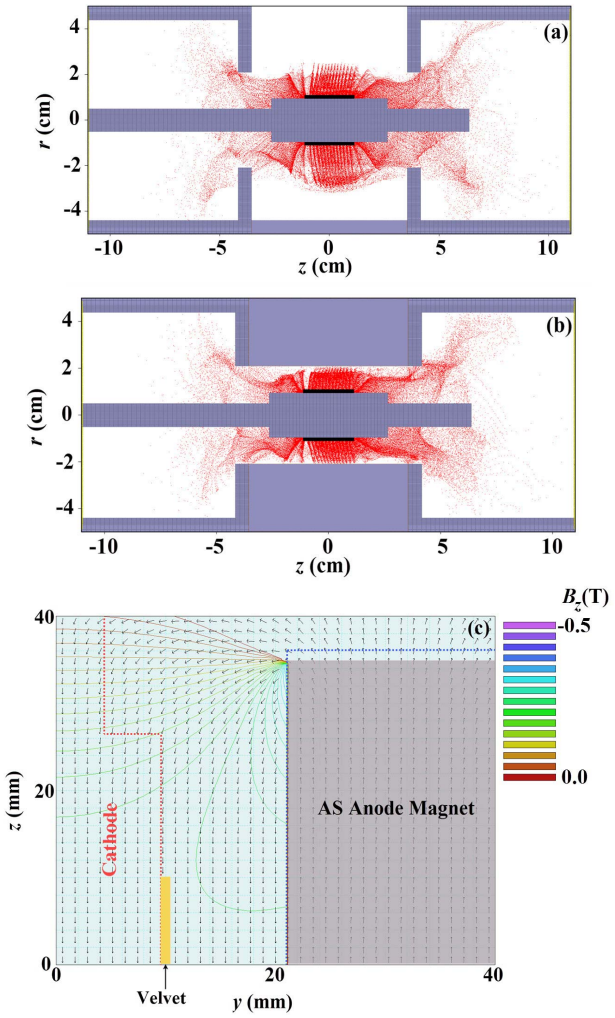

Fig. 13. PIC calculated electron positions at 40 ns after the 10 ns rise time of the voltage along the flat top of the voltage pulse, in the coordinate space along a [z, r] plane slicing through (a) the open magnetron slot and (b) the opposite vane, under the same conditions as the experiment in Fig. 11. (c) Contours of B_z and the vector plot of the magnetic field orientation for six AS magnets (gray shaded area) and the cathode seen in Fig. 11(a). Red dotted and blue lines: cathode and anode surfaces, respectively. Yellow box: velvet emitter.

The resulting microwave power [Fig. 12(a)] settles at ∼15 MW, that is, ∼7 MW when we take into account the reduction of the power in the experimental waveguide. This value compares well with the experiment. The difference between the total current and the magnetron current is the current which does not contribute to microwave generation. The total current corresponds to a value between that seen in Fig. 11(c) and (d). The frequency [Fig. 12(b)] shows some mode competition with two dominating frequencies, ∼2.8 and 2.4 GHz. Mode competition was observed experimentally too, but the registered dominant frequency was at 2.57 GHz and at lower amplitude, 2.72 GHz. This difference could be the result of the interaction of the waveguide attached to the open magnetron slot interacting with the magnetron and which is not modeled in this simulation.

In Fig. 13(a) and (b) ($B_R = 1.2$ T), in contrast to Fig. 10(a) and (b) ($B_R = 1.7$ T), the electron flow exits the magnetron at both ends as an axial current which allows the power to grow. In Fig. 13(c), contours of the magnitude of B_z and the direction of the magnetic fields are drawn. These correspond to the edge electron motion seen in Fig. 13(a) and (b). [Note in Fig. 13(a) and (b), the distinct radial electron motion starting from emission mesh points along the emitter surface. Here, the radial motion is more pronounced than the axial flow. In other cases, (i.e., Fig. 10), the axial blurs the radial flow.]

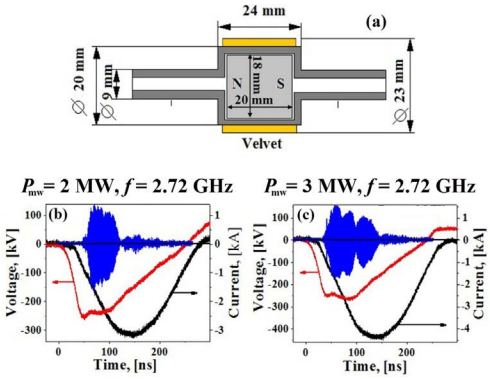

Fig. 14. (a) Geometry of the cathode used in this experiment. Six AS magnets are present and a 20-mm long, 18-mm diameter magnet is inserted in the cathode. The velvet emitter length $l_e = 20$ mm. Waveforms of the current, voltage, and microwave power for (b) $\varphi_{ch} = 1.9$ kV and (c) $\varphi_{ch} = 2.3$ kV.

D. Experiments With AS Magnets and Short Cathode Magnets

In Fig. 14, we show the measured waveforms of the current, voltage, and microwave pulse for different values φ_{ch} for a short [24-mm long, see Figs. 3(d) and 14(a)], 20-mm diameter cathode containing an 18-mm diameter and 20-mm long magnet rod. This setup results in the generation of microwaves not exceeding a few megawatts of power during ≤70 ns. Here again, increasing the charging voltage 1.4 times changes the voltage very little but leads to a drastic increase in the current up to 4.3 kA which is almost the short-circuit mode of the LIA operation for this charging voltage.

In Fig. 15(a), the large step, ~ -0.4 T, is the contribution of the cathode magnet. Near the poles of this magnet, B_z reduces to ~ -0.2 T which decreases again near the poles of the AS magnets. On the other hand, large radial components pointing toward the cathode form too close to the poles of the cathode magnet. This behavior is seen clearly in the magnetic field vector plot in Fig. 15(b), which one should compare to Fig. 13(c), where no cathode magnet is present. The large radial component of the magnetic field near the poles of the cathode magnet results in the localization of electrons near these poles with some of the electrons escaping as axial current [Fig. 15(c) and (d)].

In Fig. 16(a), the PIC calculated time dependence of the voltage, total, and magnetron currents and the microwave power are drawn, while in Fig. 16(b), the frequency–time analysis of the electric field at the edge of the conical antenna is presented, both for the experimental conditions in Fig. 14. For almost the same voltage, the total calculated current is considerably lower than the experimental value. The calculated microwave power is though considerably higher than that measured experimentally (even if the antenna/waveguide ratio is taken into account). The calculated power is higher than

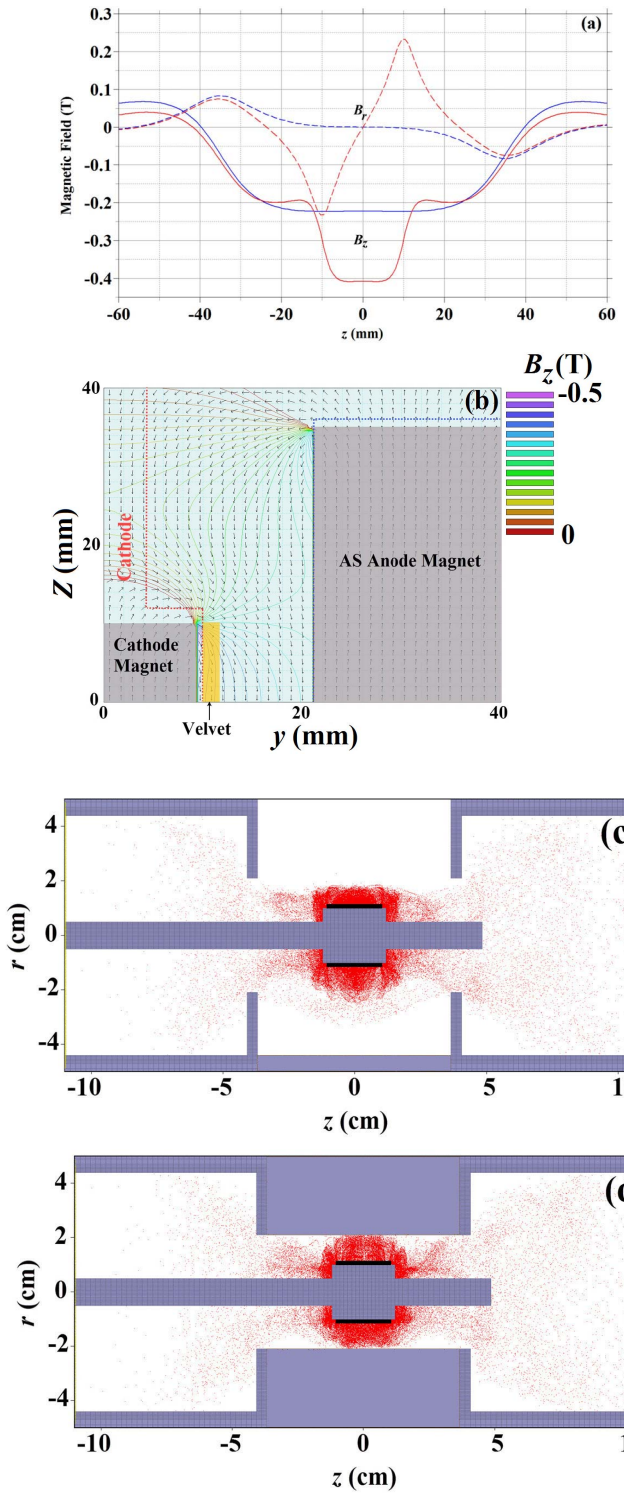

Fig. 15. (a) Axial (B_z—solid lines) and radial (B_r—dashed) components of the magnetic field along a line at $r = 11.5$ mm (the surface of the velvet emitter) with a cathode magnet as in Fig. 14(a) (red) and without it (blue). (b) Same as Fig. 13(c) for the short cathode and its magnet. (c) and (d) PIC calculated electron positions at 40 ns after the 10-ns rise time along the flat top of the voltage pulse, in the coordinate space along [z, r] planes slicing through the same surfaces as in Fig. 13(a) and (b).

that of the previous case (Fig. 13), probably because of the higher magnetic field in the interaction region, but the experimental power (Fig. 14) is low. We have no explanation for this, apart from increased losses of electrons moving

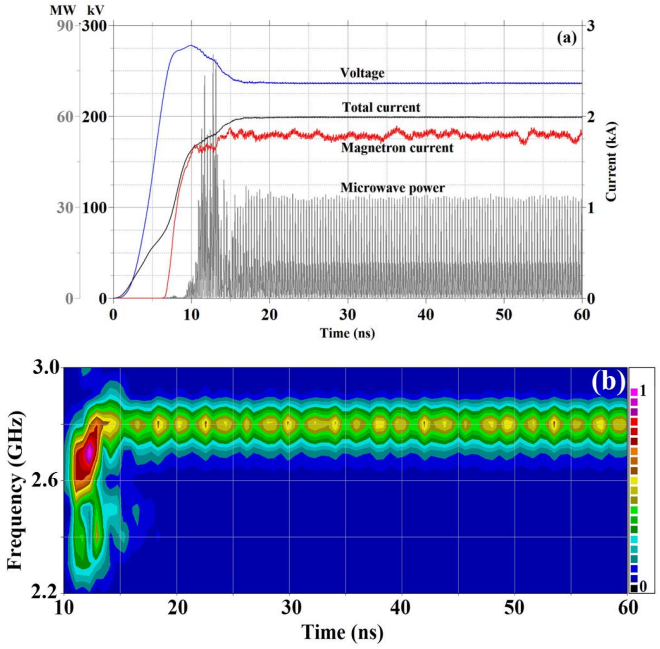

Fig. 16. (a) PIC calculated time dependence of the voltage, total and magnetron currents, and the mw power versus time. (b) Frequency–time analysis of the electric field at the edge of the conical antenna for the experimental conditions as in Fig. 14.

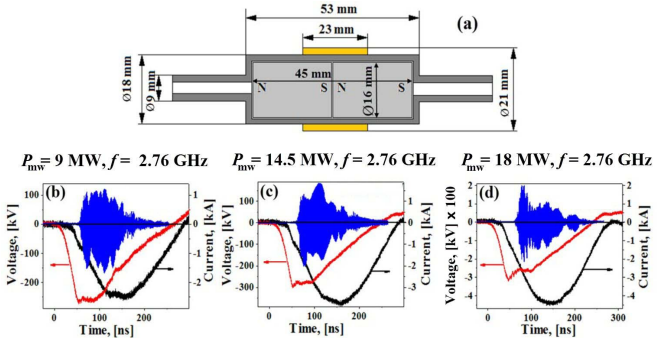

Fig. 17. (a) Geometry of the cathode used in this experiment. Six AS magnets are present and a 45-mm long, 16-mm diameter magnet is inserted in the cathode. The velvet emitter length $l_e = 23$ mm. Waveforms of the current, voltage, and microwave power for (b) $\varphi_{ch} = 1.5$ kV, (c) 1.9 kV, and (d) 2.3 kV.

toward the cathode holder along the magnetic field lines near the poles of the cathode magnet not taken into account in the calculations. These electrons can produce surface plasma quickly propagating along the B_z magnetic lines and serving as a source of electrons crossing the gap toward the anode along the B_r magnetic lines near the AS magnet poles. The large current is evidence for such electron losses which can cause misleading results.

E. Experiments With AS Magnets and Long Cathode Magnets

In an attempt to decrease electron losses, we chose the cathode seen in Fig. 17. A 16-mm diameter, 45-mm long magnet was inserted into the hollow body of this cathode [see Fig. 3(e)]. For this arrangement, we obtained the highest microwave peak power up to ~20 MW [Fig. 17(d)] and longer pulses (~110 ns). However, the current continued to increase and considerably, as the charging voltage, φ_{ch}, was increased.

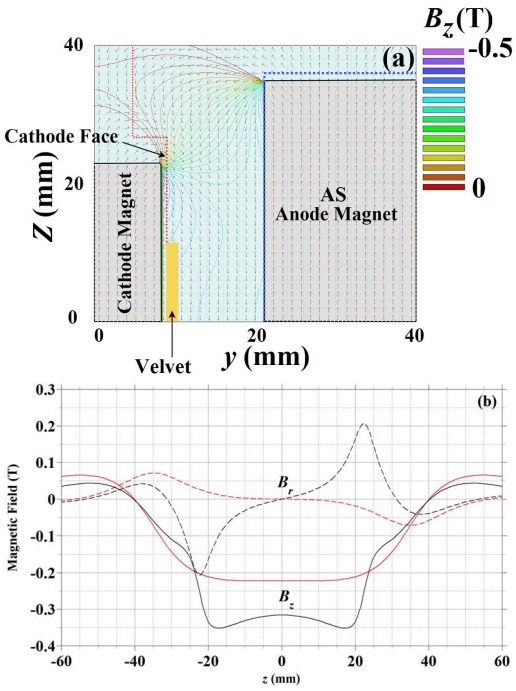

Fig. 18. (a) Contours of B_z and the vector plot of the magnetic field orientation for six AS (gray shaded area) and the cathode seen in Fig 17(a). (b) Axial (B_z—solid lines) and radial (B_r—dashed) components of the magnetic field along a line at $r = 10.5$ mm for AS magnets only (red) and the additional cathode magnet of Fig. 17(a) (black).

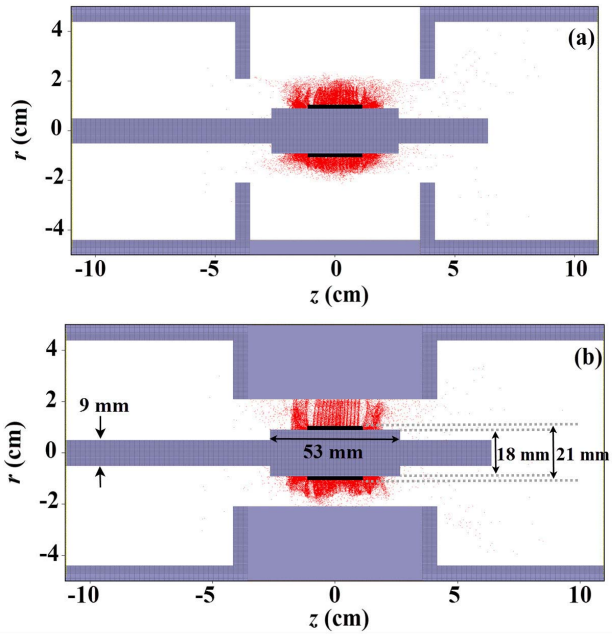

Fig. 19. PIC calculated electron positions at 40 ns after the 10-ns rise time of the voltage along the flat top of the voltage pulse, in the coordinate space along [z, r] planes. (a) and (b) are the same views as in Fig. 13(a) and (b), respectively, for the dimensions as in Fig. 17(a) and magnetic fields as in Fig. 18.

In Fig. 18(a), the contours of the axial magnetic field component and the vector plot of the magnetic field for six AS magnets and the cathode magnet of Fig. 16 are drawn. The pole of the cathode magnet here is moved away from the emission region edge (compare with Fig. 15). Nevertheless, the radial component due to the cathode magnet poles affects

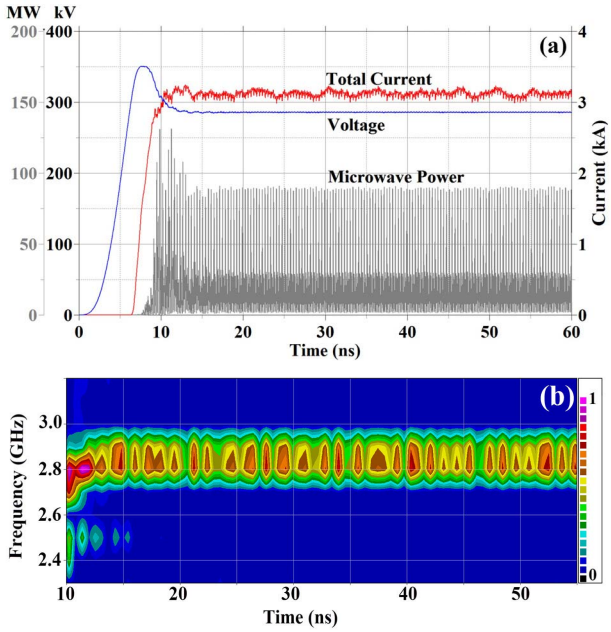

Fig. 20. (a) PIC calculated time dependence of the voltage, total current, and the mw power versus time. (b) Frequency–time analysis of the electric field at the edge of the conical antenna for the experimental conditions in Fig. 17.

electrons before they can reach the region of anode magnet poles [Fig. 18(b)]. The axial magnetic field amplitude is considerably higher with the addition of the cathode magnet but lower than for the short cathode magnet in Fig. 15(b).

In Fig. 19, the axial electron flow leaving the interaction region or that collected on the anode caps is small in comparison to both cases seen in Figs. 15 and 13. The resulting voltage, current, and microwave power are drawn in Fig. 20(a), while the frequency–time analysis is shown in Fig. 20(b).

The simulated power settles at the instantaneous value of ~90 MW compared to the experimentally measured ~40 MW (the value in Fig. 17(c) multiplied by the antenna/waveguide factor of 2.2). In all our experimental measurements, the current increases during the period when the voltage is constant [i.e., Fig. 20(a)]. This we relate to our earlier observations of the cathode plasma which though does not shorten the cathode-anode gap but expands a distance of the order of ~1 mm [17]. This shortens the gap and causes the current to increase. If the current increases while the voltage decreases, it is due to processes such as uncontrolled electron losses between the cathode and the anode away from the initial emission region.

IV. Conclusion

We have carried out an experimental and numerical research of a relativistic A6 magnetron with a single microwave power radial output using anode segment shaped permanent magnets inside the anode vanes and rod magnets inserted in the cathode. It is shown that it is possible to operate this compact magnetron with modern (NdFeB) permanent magnets to obtain microwave power of several tens of megawatts and $\sim 10^{-7}$ s long pulses. In the present design, the electronic efficiency of the microwave radiation was $\leq 7\%$. The experimental efficiency is limited by electron losses along the cathode surface where explosive emission plasma forms along points where the

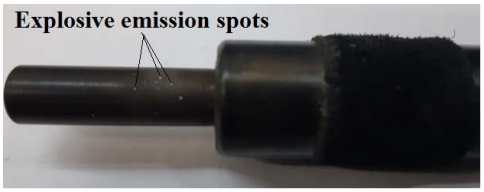

Fig. 21. Visible discharge points along the cathode holder surface far from the velvet.

axial magnetic field is no longer present. This seems to occur in most cases studied when the charging voltage is elevated. In order to avoid this effect, we tested cathodes with 90-μm thick Al_2O_3 hard coating increasing the electrical breakdown strength up to 300 kV/cm [18]. Nevertheless, these experiments also showed an increase in magnetron current similar to that obtained in the absence of cathode coating. Visual inspection of hard anodized cathodes after their operation showed the damage of the coating near the poles of the AS magnets, i.e., where the magnetic field lines cross the anode-cathode gap (see Fig. 21). This damage can be related to the charging of the thin Al_2O_3 ceramic surface by electron flow and as well as to the possible ion flow generated by the anode plasma leading to either surface or bulk electrical breakdowns. The latter leads to the formation of the plasma serving as a source of electron emission toward the anode at locations where magnetic field lines cross the cathode-anode gap.

Our simulations also show that the magnet poles affect the electron dynamics when these are close to the interaction region. We intend to find ways to optimize the dynamics for best performance. Namely, to avoid these plasma spots to form along the cathode holder, the permanent magnets should provide an axially uniform magnetic field not only within the anode–cathode volume but also down- and up-stream from this region. However, increasing the magnet length decreases the magnetic field in the center. There are ways to overcome this limitation when using permanent magnets. One such way, which we shall consider in the near future, is to reduce the volume of the magnetron.

ACKNOWLEDGMENT

The authors would like to thank Y. Bliokh for fruitful discussions; A. Sayapin who carried out preliminary research of the magnetron with inserted rod magnets; and V. Goloborodko, S. Gleizer, E. Flyat, and H. Shannan for technical assistance.

REFERENCES

[1] J. Benford, J. A. Swegle, and E. Schamiloglu, *High Power Microwaves*, 3rd ed. Boca Raton, FL, USA: CRC Press, 2015.

[2] R. M. Gilgenbach, R. J. Barker, N. C. Luhmann, J. H. Booske, and G. S. Nusinovich, "Crossed-field devices," in *Modern Microwave and Millimeter-Wave Power Electronics*. Piscataway, NJ, USA: IEEE Press, 2004.

[3] G. A. Mesyats, *Explosive Electron Emission*. Yekaterinburg, Russia: URO, 1998.

[4] M. I. Fuks and E. Schamiloglu, "70% efficient relativistic magnetron with axial extraction of radiation through a horn antenna," *IEEE Trans. Plasma Sci.*, vol. 38, no. 6, pp. 1302–1312, Jun. 2010.

[5] M. Fuks and E. Schamiloglu, "Rapid start of oscillations in a magnetron with a 'transparent' cathode," *Phys. Rev. Lett.*, vol. 95, no. 5, Nov. 2005, Art. no. 205101.

[6] Y. E. Krasik *et al.*, "Study of electron diodes with a ferroelectric plasma cathode," *IEEE Trans. Plasma Sci.*, vol. 28, no. 5, pp. 1642–1647, Oct. 2000.

[7] A. Sayapin, A. L. Levin, U. Dai, and Y. E. Krasik, "Stabilized operation of a microwave compressor driven by relativistic S-band magnetron," *IEEE Trans. Plasma Sci.*, vol. 42, no. 12, pp. 3961–3967, Dec. 2014.

[8] I. Schnitzer, A. Rosenberg, C. Leibovitz, C. Cohen, M. Botton, and J. Leopold, "Evolution of spectral power density in grounded-cathode relativistic magnetron," *Proc. SPIE*, vol. 2843, Oct. 1996, pp. 101–109.

[9] W. Li, J. Zhang, Z.-Q. Li, and J.-H. Yang, "A portable high power microwave source with permanent magnets," *Phys. Plasmas*, vol. 23, no. 6, Jun. 2016, Art. no. 063109.

[10] A. J. Sandoval, "Experimental verification of A6 magnetron with permanent magnet," M.S. thesis, Dept. Elect. Eng., Univ. New Mexico, Albuquerque, NM, USA, May 2018. [Online]. Available: http://digitalrepository.unm.edu/ece_etds/400

[11] C. Leach, S. Prasad, M. I. Fuks, and E. Schamiloglu, "Compact relativistic magnetron with Gaussian radiation pattern," *IEEE Trans. Plasma Sci.*, vol. 40, no. 11, pp. 3116–3120, Nov. 2012.

[12] A. Sayapin and A. Levin, "Relativistic magnetron with inbuilt magnetic block," in *Proc. EUROEM Eur. Electromagn. Conf.*, Toulouse, France, Jul. 2012, p. 253.

[13] Y. Hadas, A. Sayapin, Y. E. Krasik, V. Bernshtam, and I. Schnitzer, "Plasma dynamics during relativistic *S*-band magnetron operation," *J. Appl. Phys.*, vol. 104, Sep. 2008, Art. no. 064125.

[14] A. Sayapin, A. Levin, and Y. E. Krasik, "Operation of a six-cavity *S*-band relativistic magnetron at frequencies in the range of its resonant response," *IEEE Trans. Plasma Sci.*, vol. 43, no. 11, pp. 3827–3832, Nov. 2015.

[15] J. G. Leopold, A. S. Shlapakovski, A. F. Sayapin, and Y. E. Krasik, "Pulse-shortening in a relativistic magnetron: The role of anode block axial endcaps," *IEEE Trans. Plasma Sci.*, vol. 44, no. 8, pp. 1375–1385, Aug. 2016.

[16] B. Goplen, L. Ludeking, D. Smith, and G. Warren, "User-configurable MAGIC for electromagnetic PIC calculations," *Comput. Phys. Commun.*, vol. 87, nos. 1–2, pp. 54–86, May 1995.

[17] Y. Hadas, A. Sayapin, Y. E. Krasik, V. Bernshtam, and I. Schnitzer, "Plasma dynamics during relativistic-band magnetron operation," *J. Appl. Phys.*, vol. 104, no. 8, Sep. 2008, Art. no. 064125.

[18] T. Queller, A. Shlapakovski, and Y. E. Krasik, "Plasma formation in a double-gap vircator," *J. Appl. Phys.*, vol. 108, no. 3, Nov. 2010, Art. no. 103302.